Effect of chain stiffness on the competition between crystallization and glass-formation in model unentangled polymers

Hong T. Nguyen, Tyler B. Smith, Robert S. Hoy, and Nikos Ch. Karayiannis

Citation: The Journal of Chemical Physics **143**, 144901 (2015); doi: 10.1063/1.4932193
View online: http://dx.doi.org/10.1063/1.4932193
View Table of Contents: http://scitation.aip.org/content/aip/journal/jcp/143/14?ver=pdfcov
Published by the AIP Publishing

Effect of chain stiffness on the competition between crystallization and glass-formation in model unentangled polymers

Hong T. Nguyen,[1] Tyler B. Smith,[1] Robert S. Hoy,[1,a)] and Nikos Ch. Karayiannis[2]
[1]*Department of Physics, University of South Florida, Tampa, Florida 33620, USA*
[2]*Institute for Optoelectronics and Microsystems (ISOM) and ETSII, Polytechnic University of Madrid, Madrid, Spain*

(Received 18 June 2015; accepted 14 September 2015; published online 8 October 2015)

We map out the solid-state morphologies formed by model soft-pearl-necklace polymers as a function of chain stiffness, spanning the range from fully flexible to rodlike chains. The ratio of Kuhn length to bead diameter (l_K/r_0) increases monotonically with increasing bending stiffness k_b and yields a one-parameter model that relates chain shape to bulk morphology. In the flexible limit, monomers occupy the sites of close-packed crystallites while chains retain random-walk-like order. In the rodlike limit, nematic chain ordering typical of lamellar precursors coexists with close-packing. At intermediate values of bending stiffness, the competition between random-walk-like and nematic chain ordering produces glass-formation; the range of k_b over which this occurs increases with the thermal cooling rate $|\dot{T}|$ implemented in our molecular dynamics simulations. Finally, values of k_b between the glass-forming and rodlike ranges produce complex ordered phases such as close-packed spirals. Our results should provide a useful initial step in a coarse-grained modeling approach to systematically determining the effect of chain stiffness on the crystallization-vs-glass-formation competition in both synthetic and colloidal polymers. © *2015 AIP Publishing LLC.* [http://dx.doi.org/10.1063/1.4932193]

I. INTRODUCTION

Understanding crystallization of synthetic polymers is one of the most longstanding and difficult problems in chemical engineering, materials science, and soft matter physics.[1,2] Crystallization from dense polymer melts is kinetically limited by slow processes such as lamella-formation and the slow microscale dynamics of the constituent entangled chains;[2,3] such factors produce correspondingly slow phase transition kinetics and strong preparation-history-dependence of the final crystalline morphology. For many technologically important polymers, the same slow processes produce glass-formation under thermal cooling, making crystallization difficult to achieve on experimentally accessible time scales. This complexity makes formulation of predictive analytic models very difficult.[4,5]

Given the difficulties inherent to both experimental and analytic approaches, simulations provide an excellent tool for improving our understanding of polymer solidification. Crystallization, glass-formation, and the competition between them can be readily studied by varying sample preparation protocol (e.g., the thermal cooling rate $|\dot{T}|$). Chemically detailed, atomistic or united-atom models[6–9] exhibit crystallization[8–10] as well as glass formation,[11] and incorporate the 3– and 4–body (bending and torsion) interactions required to produce realistic crystalline morphologies. Recent studies of the "CG-PVA" model (a united-atom, coarse-grained model for polyvinyl alcohol)[12–15] have provided significant insights into poorly understood effects such as the asymmetry between crystallization and melting, and the role played by chain disentanglement during cooling from dense melts. However, the generality of results obtained with the CG-PVA (or any other chemically specific) model remains unclear.

Fortunately, studies employing coarse-grained models can shed light on universal aspects of the crystallization process. Simple polymer models that possess four key features: (i) the soft excluded volume and van der Waals interactions necessary to capture thermal behavior (e.g., temperature-controlled phase transitions), (ii) variable chain stiffness, (iii) local chain structure that is amenable to crystallization, and (iv) a simple, well-defined ground-state crystal, should be of particular value. The simplest models, which treat polymers as chains of tangent hard spheres,[16–18] lack (i) and often (ii). The widely used Kremer-Grest bead-spring model (KG)[19] possesses features (i) and (ii) but not (iii) and (iv), since crystallization is effectively suppressed by the incommensurability of its monomer diameter and covalent backbone bond length.[20] However, a recently introduced simple modification of KG removes this incommensurability and includes all four features.[21]

The main goal of this study is to examine the role chain topology and flexibility (or equivalently stiffness) plays in controlling solidification, i.e., crystallization vs. glass-formation, in model polymers. Rather than studying a large number of chemically realistic models with different pair, bond, and angular interactions and crystalline structures, we employ a single model[21] with a single, continuously adjustable parameter (bending stiffness k_b) and a single, well-defined crystalline ground state, to isolate the role that angular stiffness plays in this competition. This latter approach is naturally well suited to studying polymer solidification in parametric fashion.

a)Electronic address: rshoy@usf.edu

Our model[21] is *not* designed to capture the complex crystal structures formed by typical synthetic polymers (e.g., PE, PP, and PVA), and we do not claim that it predicts the crystal structure for any single polymer chemistry. However, it *is* designed to efficiently capture general *trends* in polymer solidification. In this paper, we focus on how the solidification process varies with chain stiffness when all other control variables are held fixed. Such general trends can, at least in principle, be observed in experiments conducted across *families* of synthetic polymers, e.g., families in which chain stiffness can be varied (without significantly changing chemical composition) by varying side chain density.[22] Similar considerations have motivated recent experimental studies of *colloidal* polymers (CPs).[23–29] Such experiments have proven useful for explaining trends, e.g., the variation of glass transition temperature T_g with chain length N in typical amorphous synthetic polymers.[25] With respect to its applicability to microscopic polymers, the present paper is similar in spirit to Ref. 25, but with a greater focus on semicrystalline systems. We will argue below that another strength of our model is its applicability to predicting the structure of CPs.

We perform extensive molecular dynamics (MD) simulations to determine how melts of various k_b (spanning the entire range from the fully flexible to the rodlike limits) solidify during cooling and identify the factors controlling their crystallization, glass-formation, and the competition thereof. To eliminate slow crystallization kinetics arising from slow melt dynamics (e.g., reptation[3]), we focus in this initial study on unentangled chains. Through these simulations, we identify how characteristic features of the solidification process vary with k_b and thus isolate the effect of chain stiffness on the morphologies formed during cooling from dense melts.

We find a complex dependence of solid-state morphology on k_b and explain it primarily in terms of the variation of Kuhn-segment-scale structure with k_b. In the flexible limit ($l_K \simeq r_0$), monomers occupy the sites of close-packed (face centered cubic (FCC) or hexagonal close packed (HCP)) crystallites, but chains possess random-walk-like structure. In the rodlike limit ($l_K \gg r_0$), monomers again close-pack, but chains form nematic domains with a single, well-defined orientation. For intermediate bending stiffness, systems possess chain-scale ordering intermediate between isotropic and nematic and form solids that are highly disordered at the monomer level, i.e., are good glass-formers. Neither intermediate values of l_K/r_0 nor intermediate-scale nematic order seem to be compatible with close-packing; glass formation is associated with the resulting geometric frustration. We also report complex multidirectional-nematic and spiral morphologies that coexist with locally close-packed order.

II. MODEL AND METHODS

A. Interaction potential and MD simulation protocol

Our simulations employ the semiflexible version of the soft-pearl-necklace polymer model described at length in Ref. 21. It is comparable to the Kremer-Grest bead-spring model[19] but possesses crystalline ground states since the equilibrium backbone bond length ℓ_0 is commensurate with the equilibrium monomer diameter r_0, i.e., the condition $\ell_0 = r_0$ is amenable to formation of close-packed crystals. All monomers have mass m and interact via the truncated and shifted Lennard-Jones potential,

$$U_{LJ} = 4\epsilon\left[\left(\frac{\sigma}{r}\right)^{12} - \left(\frac{\sigma}{r}\right)^{6} - \left(\frac{\sigma}{r_c}\right)^{12} + \left(\frac{\sigma}{r_c}\right)^{6}\right], \quad (1)$$

where ϵ is the intermonomer binding energy and r_c is the cutoff radius. Attractive van der Waals interactions are included by setting $r_c = 2^{7/6}$ (in LJ units). The MD time step used here is $\delta t = \tau/200$, where τ is the Lennard-Jones time unit $\sqrt{ma^2/\epsilon}$.

Bonds between adjacent beads along the chain backbone are modeled using the harmonic potential,

$$U_c(\ell) = \frac{k_c}{2}(\ell - a)^2, \quad (2)$$

where ℓ is bond length, a is monomer diameter, and $k_c = 600\epsilon/a^2$ is the bond stiffness. To produce polymer chains with $\ell_0 = r_0 = a$, we set $\sigma = 2^{-1/6}a$. For this pair of k_c and σ, the energy barrier for chain crossing is at least $50k_BT$ over the whole temperature range considered herein.

Bending stiffness is included using the standard potential[30]

$$U_b(\theta) = k_b(1 - cos(\theta)), \quad (3)$$

where $cos(\theta_i) = (\vec{b}_i \cdot \vec{b}_{i+1})/(\|\vec{b}_i\|\|\vec{b}_{i+1}\|)$ and the bond vector $\vec{b}_i = \vec{r}_{i+1} - \vec{r}_i$ has $\|\vec{b}_i\| = \ell_i$. We study systems with $0 \le k_b \le 12.5\epsilon$, and show below that the upper part of this range yields rod-like chains that order nematically.

All systems are composed of $N_{ch} = 500$ chains. Periodic boundaries are applied along all three directions of cubic simulation cells. In this study, we focus on polymers with chain lengths $N = 13$, 25, and 50 and compare them to results for monomers. These chains are either unentangled or (for $N = 50$) very weakly entangled.[31] Initial systems are generated by placing randomly oriented random-walk-like coils within dilute cells. Systems are then thoroughly equilibrated at temperatures (monomer number densities) $k_BT/\epsilon = 1.2$ ($\rho = 1.0a^{-3}$) for $k_b < 7\epsilon$, $k_BT/\epsilon = 1.4$ ($\rho = 0.9a^{-3}$) for $7\epsilon \le k_b < 10\epsilon$, and $k_BT/\epsilon = 1.6$ ($\rho = 0.8a^{-3}$) for $k_b \ge 10\epsilon$, i.e., well above the k_b-dependent solidification temperatures reported below. To avoid any artifacts arising from insufficient equilibration, we monitor the chain statistics $\langle R^2(n)\rangle$ and check for convergence at all chemical distances n.[30] Systems are then further equilibrated at constant (zero) pressure and then cooled to $T = 0$ (also at zero pressure) at a rate $|\dot{T}|$. Pressure is controlled using a Nose-Hoover barostat. To examine the dependence of solid-state ordering upon the cooling (quench) rate, we consider $|\dot{T}|$ ranging from $10^{-6}/\tau$ to $10^{-4}/\tau$. All MD simulations are performed using LAMMPS.[32]

B. Measures of monomer- and chain-scale order

During cooling, we monitor several metrics quantifying local (monomer-scale) and global (chain-scale and above) structures. Since U_{LJ} is attractive and we perform simulations at zero pressure, all systems densify with decreasing T. We report the monomer densities $\rho(T)$ in terms of the

packing fraction $\phi = \pi\rho/6$. Since U_{LJ} is a "soft" potential and solidification occurs at rather high T, and to aid comparison with results for other models including athermal (hard-sphere) systems (e.g., Refs. 33–35), we also report values of the *effective* (thermalized[36]) packing fraction at solidification: $\phi_s^{eff} = \pi\rho_s^{eff}/6$, where $\rho_s^{eff} = \rho(r_s^{eff})^3$, and the effective monomer radius r_s^{eff} is the smallest real solution to[37]

$$U_{LJ}(r_s^{eff}) - U_{LJ}(r_0) = 1.1 k_B T_s, \tag{4}$$

where T_s is the temperature at solidification, identified as described in Section III B.

Local structure at the monomer level is identified through the characteristic crystallographic element (CCE) norms.[33–35,38] The CCE-based analysis employs descriptors that quantify the orientational *and* radial similarities of a given monomer's local environment to that of various "reference" structures such as HCP and FCC crystals, and is in most cases[38] a sharper discriminator of local crystalline order than the commonly used Steinhardt bond-orientational-order (BOO) metrics.[39] CCE norms are built around the defining set of crystallographic elements and the subset of distinct elements of the corresponding point symmetry groups that uniquely characterize the reference crystal structure. For example, the FCC crystal symmetry is mapped onto a set of four three-fold axes (roto-inversions of $2\pi/3$), while the HCP is mapped onto a single six-fold symmetry axis (roto-inversion of $\pi/3$). A scan in the azimuthal and polar angles identifies the set of axes that minimize the CCE norm of a reference site (atom or particle) with respect to a given crystal structure X. Details on the underlying mathematical formulae and the algorithmic implementation can be found in Ref. 38. Once the CCE norm (ϵ_i^X) is calculated for each site i, the 'X-like' monomer fraction f_X is identified as the fraction of sites for which ϵ_i^X is less than a preset threshold value. Here, CCE norms are calculated with respect to the FCC and HCP crystals, and the fivefold local symmetry.

Multiple measures are used to characterize nematic order. The polymers' persistence length,[40]

$$l_p = \sum_{i=0}^{N-2} \vec{b}_i \cdot \vec{b}_{i+1}, \tag{5}$$

measures how single-chain conformations change with T. Average nematic order at the *chain* level is characterized via the method employed in Ref. 40: alignment of chains can be characterized by the largest eigenvalue S_g of the tensor $Q_{\alpha\beta}$ which is defined by

$$Q_{\alpha\beta} = \left\langle \frac{3}{2}\hat{u}_{j\alpha}\hat{u}_{j\beta} - \frac{1}{2}\delta_{\alpha\beta} \right\rangle, \tag{6}$$

where $\hat{u}_j$ is the end-to-end unit vector of chain j, δ is the Kronecker delta, and α, β denote the Cartesian directions x, y, z, and the average is taken over all chains in the system. By construction, $S_g = 1$ signifies perfect alignment of all chains. In contrast, $S_g = 0$ means random orientation.

Nematic order at the *bond* level is characterized via the method employed in Ref. 14: tensor order S is given by

$$S = \sqrt{\frac{3}{2}\mathrm{Tr}(q^2)},\ q_{\alpha\beta} = \left\langle \hat{b}_\alpha \hat{b}_\beta - \frac{1}{3}\delta_{\alpha\beta} \right\rangle. \tag{7}$$

Here, Tr is the trace operator, $\langle \cdots \rangle$ denotes the average over all normalized bond vectors $\mathbf{b}$ in each sub-cell, and $\hat{b}_\alpha$ and $\hat{b}_\beta$ are Cartesian components of $\mathbf{b}$. In Equation (7), $S = 1$ corresponds to perfect alignment of bonds in a given subcell and $S = 0$ corresponds to random bond orientation within that subcell. In order to get a single number for the average bond orientation in the system, we average S over all subcells in the simulation.[41] While the average tensor order defined in this way depends on the size of the subcells used, we have tested different grid sizes and found that the results presented below are qualitatively unaffected by small changes when the subcell size is 2-3 monomer diameters.

Another measure of nematic order at the bond level is provided by the bond-orientational correlation function

$$F_{bb}(\Delta) = \left\langle \left| \vec{b}_i(\vec{R}_i) \cdot \vec{b}_j(\vec{R}_i + \vec{\Delta}_{ij}) \right| \right\rangle - \frac{1}{2}, \tag{8}$$

a sensitive measure of long-range nematic order that is positive when bond vectors separated by a distance Δ are correlated, and zero when they are uncorrelated. Here $\vec{b}_i = \vec{r}_{i+1} - \vec{r}_i$ as defined above, $\vec{R}_i = (\vec{r}_{i+1} + \vec{r}_i)/2$ indicates the midpoint of this bond, $\vec{\Delta}_{ij} = \vec{R}_j - \vec{R}_i$, and the brackets denote averages over all $j > i$.

C. Distinction from previous modeling efforts

The Kremer-Grest bead-spring model has long been used to study the polymeric glass transition.[20] In the original KG model[19] and subsequent modifications,[42,43] the equilibrium backbone bond length ℓ_0 is different from the equilibrium non-bonded separation r_0; the resulting length scale competition was shown in Refs. 20, 42, and 43 to suppress crystallization.[44,45] Our model sets $\ell_o = r_o$ and therefore possesses a simple (close-packed) crystalline ground state. However, it also displays glass-formation under thermal quenches at sufficiently large $|\dot{T}|$[21] and is therefore well suited to studies of competing crystallization and glass transitions.

Another class of polymer model that has been extensively used to study solidification, but from which ours is crucially different, is that of tangent hard spheres (THS). THS polymers may be either flexible (freely-jointed),[16,17] semiflexible,[18] or partially flexible.[46–48] They are *athermal* since monomers interact via purely repulsive (hard-sphere) pair potentials. Several recent studies of flexible chains have examined the CF-vs-GF competition in terms of the effects of varying chain length N and monomer density ρ.[34,35,49–51] These found an entropically (free volume) driven transition from a disordered fluid state to a close-packed (FCC or HCP) crystal as ρ increases, that is, however, increasingly prone to kinetic suppression by jamming as N increases. While such results should be useful in understanding the structure of polymeric solids at low T, the athermal nature of the model may limit their applicability to typical synthetic polymers, for which thermal fluctuations (k_BT) play a dominant role at typically encountered $T \sim T_{room}$.

THS models usually fix $l_o = r_o$ through holonomic constraints rather than the relatively "soft" harmonic potential (Eq. (2)) used herein. Relaxation of the $\ell_0 = r_0$ condition[51] has been shown to profoundly affect THS crystallizability,

in particular, by allowing fluctuations of ℓ that speed its dynamics[51] or by changing the ground state's order by imposing $\ell_0 \neq r_0$.[52] In contrast, our model allows significant thermal fluctuations of both ℓ_0 and r_0,[21] and thus applies $\ell_0 = r_0$ only in a thermodynamically averaged sense.

MD simulations similar to those employed here have long been used to examine ordered morphologies formed during thermal quenching of model polymeric systems; see e.g., Refs. 8, 9, 13, 15, and 53. Vettorel *et al.*[53] employed very similar simulations to study the "phase diagram" of CG-PVA; Figure 1 of Ref. 53 is very similar to our Figure 8. As described above, a key difference between the present study and previous studies of finer-grained models is that the latter employ fixed interaction potentials (usually producing relatively stiff chains), whereas here we vary chain stiffness over the entire range from fully flexible to rodlike via the parameter k_b.

III. RESULTS

For finite k_b, the ground state of our model is nematic and close-packed (NCP), i.e., monomers are close-packed into a FCC crystal and all bonds are aligned along one of the FCC Bravais lattice vectors. NCP crystals minimize each energetic term (Eqs. (1)–(3)). In this section, we will first analyze the crystallization-vs-glass-formation competition displayed by our model in terms of the k_b-dependent extent to which systems do or do not reach these ground states under thermal cooling. We will show that this extent depends sharply and nontrivially upon k_b and preparation protocol (i.e., varying $|\dot{T}|$) and relate the former dependence to how multiple measures of local and long-range structural order evolve during cooling. For example, we will show that crystallization is hindered when typical bond and torsion angles are incompatible with close-packing and also hindered when nematic order is intermediate-ranged (but not long-ranged) at temperatures slightly above T_s. We will also report effective solidification densities $\phi_s^{eff}(k_b)$ that may be used to facilitate comparisons of our results to systems with different interaction potentials. Finally, we will discuss the various k_b-dependent solid-state morphologies formed during cooling at low $|\dot{T}|$, and present a nonequilibrium "phase" diagram relating T_s and morphology to k_b.

A. Preparation-protocol dependence

Real synthetic polymers often glass-form. This may be due either to geometrical factors such as incommensurability of their bond length and monomer diameter, or to details of the protocol with which they are prepared. While our model is commensurable and possesses crystalline ground states, MD simulations show that the morphologies formed during solidification are strongly preparation-protocol dependent.

Figure 1 shows results for the close-packed monomer fraction f_{cp}, which is the sum of the HCP- and FCC-like site fractions, in the ($T = 0$) end states of cooling simulations performed over a range of rates $10^{-4}/\tau \leq |\dot{T}| \leq 10^{-6}/\tau$. These results illustrate two key features of our model and

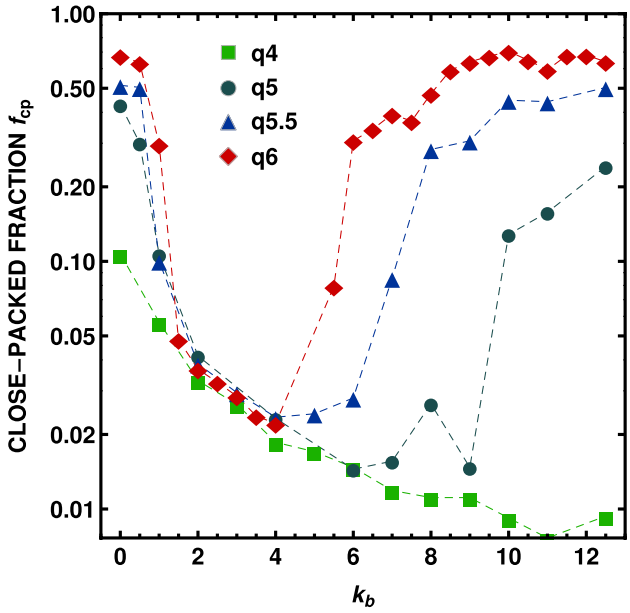

FIG. 1. Quench rate dependence of f_{cp} values in the $T = 0$ end states of cooling runs for all $N = 25$ systems. In the legend, "qx" indicates $|\dot{T}| = 10^{-x}/\tau$.

simulation method. First, the "critical" cooling rates below which we obtain a large f_{cp} vary dramatically, and in complex, nonmonotonic fashion, with k_b. Second, for all studied k_b, the variation in the obtained morphology is significant over the range of rates considered here. In other words, the data show that values of f_{cp} at fixed k_b vary differently with $|\dot{T}|$; while all decrease with increasing $|\dot{T}|$, the strength of this decrease is highly k_b-dependent.

The lowest feasible cooling rate ($|\dot{T}|$), given current computational limitations, is 10^{-6}. As illustrated in Fig. 1, this rate produces a remarkably strong k_b dependence. Maximal values of f_{cp} are larger than minimal values by nearly two orders of magnitude, indicating local ordering ranging from highly crystalline to highly amorphous. As will be described below, it also yields tremendous diversity in mid- and long-range order. We therefore focus on results from $|\dot{T}| = 10^{-6}/\tau$ quenches throughout the remainder of the paper.

B. Solidification densities and temperatures

The simplest structural metric characterizing the phase behavior, and, in particular, the competition between crystallization and glass formation, is the temperature dependence of the packing fraction $\phi = \pi\rho/6$. Figure 2 shows results for $\phi(T)$ for all systems. At high T, systems show a linear increase in ϕ as T decreases, i.e., they densify with a constant thermal expansion coefficient. For most systems this increase persists until the onset of solidification, but for the stiffest systems, it is interrupted by a density increase corresponding to the isotropic-melt → nematic-melt transition (discussed further below). At the solidification temperature $T = T_s$, ϕ increases more rapidly for crystal-forming systems; this increase is a sharp, first-order-like jump for the lowest and highest values of k_b and a more gradual concave-up increase for intermediate stiffness. Glass-forming systems show a concave-down increase in $\phi(T)$. Values of T_s (to be reported below in

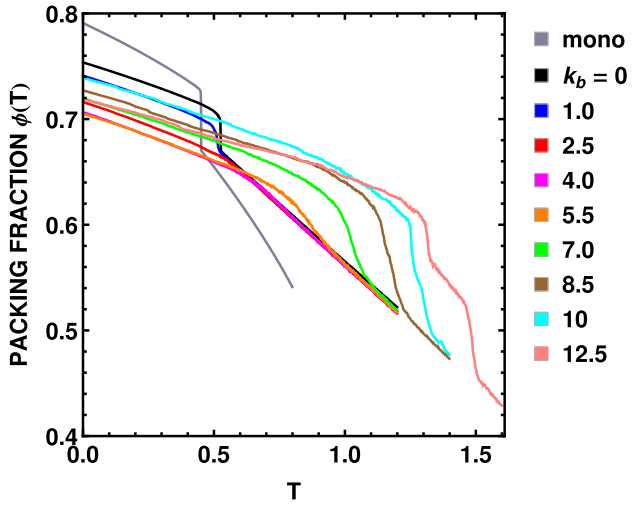

FIG. 2. Thermodynamic signatures of crystallization (or the absence of it): packing fraction $\phi(T)$ for selected $N = 25$ systems. Data for monomers ($N = 1$) are included for comparison.

Fig. 8) are identified with first-order like jumps or the points of inflection of $\phi(T)$ (T_{cryst}) or the intersection of linear fits to the high-T and low-T regimes of $\phi(T)$ (T_g). Both T_{cryst} and T_g increase monotonically with increasing k_b for $k_b \gtrsim 2\epsilon$, as is expected for synthetic polymer chains of increasing stiffness.[22,54–56] Finally, after solidification, all systems again show a linear increase in ϕ as T continues to decrease towards zero.

It is interesting to examine the k_b-dependence of system densities at solidification. Values of $\phi_s(k_b) = \phi(T = T_s(k_b))$ are reported in Table I. They decrease nearly monotonically with k_b; flexible systems crystallize at $\phi_s \simeq 0.68$, glassformers solidify in the range $0.6 < \phi_s < 0.67$, and for $k_b \gtrsim 7.5\epsilon$ all systems crystallize at $\phi_s \simeq 0.58$. While this decrease is expected since rod-like particles generally jam or crystallize at lower ϕ than their spherical counterparts,[57] we are not aware of any previous studies that systematically examined solidification density as a function of chain stiffness in model polymers. We will show below that the crossover from higher to lower values of ϕ_s that occurs at $k_b \sim 6$ corresponds to the onset of local nematic order (cf. Fig. 6).

Values of ϕ_s^{eff} also decrease nearly monotonically with increasing k_b, from very slightly above the hard-sphere jamming fraction $\phi_J = 0.637$[58] to about 0.52 for rodlike chains. Studies of jamming in thermalized colloidal systems[36] have similarly found $\phi_s^{eff} \simeq \phi_J$, and that crystallization sets in as ϕ increases beyond ϕ_J. Our results for ϕ_s^{eff} should therefore be valuable in mapping results from the present soft-pearl-necklace model to those obtained in colloidal-polymer experiments (Section III F), where monomers typically interact via stiffer, shorter-ranged pair potentials.

TABLE I. Values of ϕ upon solidification for all $N = 25$ systems: $\phi_s(k_b) = \phi(T = T_s(k_b))$ and $\phi_s^{eff}(k_b)$ (Eq. (4)) for the simulations and values of T_s reported in Figure 8 (as well as similar simulations of several additional k_b). For comparison, monomers have $\phi_s = 0.6876$ and $\phi_s^{eff} = 0.650$. We estimate "error bars" on all measured quantities are of order 1%.

k_b/ϵ	ϕ_s	ϕ_s^{eff}	k_b/ϵ	ϕ_s	ϕ_s^{eff}
0	0.683	0.643	6.5	0.590	0.535
0.5	0.683	0.643	7	0.592	0.535
1	0.679	0.641	7.5	0.582	0.522
1.5	0.681	0.645	8	0.581	0.520
2	0.673	0.636	8.5	0.570	0.508
2.5	0.666	0.627	9	0.571	0.518
3	0.657	0.616	9.5	0.586	0.520
3.5	0.651	0.609	10	0.580	0.514
4	0.648	0.605	10.5	0.580	0.514
4.5	0.643	0.599	11	0.578	0.512
5	0.642	0.598	11.5	0.583	0.515
5.5	0.597	0.544	12	0.580	0.512
6	0.606	0.552	12.5	0.584	0.526

C. Local ordering from monomeric to segment scales

Next, we show that the trends in $\phi(T)$ are closely matched by corresponding ones obtained from different descriptors of local order. Figure 3 shows the T-dependent fractions $f_{cp}(T)$ and $f_{5f}(T)$ of monomers with (a) close-packed order (FCC or HCP similarities) and (b) fivefold local symmetry, as quantified by CCE analysis.[38] Note that $f_{cp}(T)$ will approach unity and $f_{5f}(T)$ will approach zero as T decreases if the system forms a perfect crystal at $T = 0$. Thus, trends in $f_{cp}(T)$ and $f_{5f}(T)$ obtained from thermal cooling simulations at finite $|\dot{T}|$ are, respectively, measures of our model's k_b-dependent crystallizability and glass-formation tendency. Recall that the latter measure (f_{5f}) has been shown in many studies of colloidal systems[59–63] to correlate well with glass-formation, i.e., large values of f_{5f} at T slightly above T_s greatly inhibit crystallization. However, such effects have not reported for model semiflexible polymers.

Systems exhibiting sharp jumps in $\phi(T)$ also show sharp jumps in $f_{cp}(T)$. For very flexible and very stiff chains, these jumps are reminiscent of first-order transitions and occur at $T = T_{cryst}$. In contrast, glassy systems (e.g., $k_b = 4\epsilon$) show a more gradual and much weaker increase and ultimately exhibit far lower ultimate values of f_{cp}. Results for $f_{5f}(T)$ display opposite trends. For glassforming systems, f_{5f} increases continuously with decreasing T, as expected in a densifying glassformer.[64] In the limit of fully flexible chains ($k_b = 0$), the sharp increase of ordered sites is accompanied by a sharp decline in the fivefold population. In contrast, for chains that order nematically, f_{5f} remains low at all T. This is expected since the hexagonal order in planes perpendicular to the nematic director field[8,9,53] suppresses fivefold order.

Simple bead-spring models like ours possess two essentially "polymeric" features controlling the crystallization-vs-glass-formation competition: topological chain connectivity/uncrossability, and angular stiffness. Here the role of chain topology is indicated by contrasting results for polymers to data for monomers presented in Figures 2 and 3. The monomeric Lennard-Jones system is well-known as an excellent crystal-former.[65,66] Monomers exhibit sharper transitions in ϕ and f_{cp}, and ultimately reach higher values of both at $T = 0$. Furthermore, they exhibit significantly lower f_{5f} as the resulting ordered morphology is an almost perfect FCC crystal. These differences arise because chain connectivity reduces

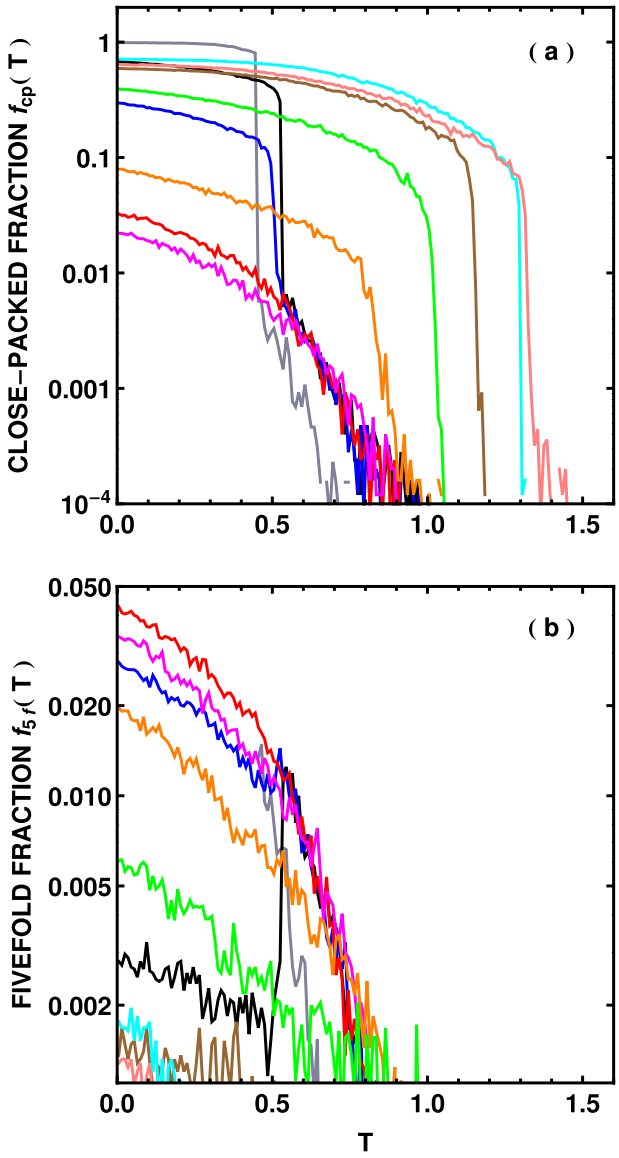

FIG. 3. Thermodynamic signatures of crystallization (or the absence of it) for selected $N = 25$ systems: (a) close-packed fraction $f_{cp}(T)$, (b) fivefold fraction $f_{5f}(T)$. Colors are the same as in Fig. 2. Note that the $T = 0$ values of f_{cp} [panel (a)] are equal to those plotted in Figure 1 (for $|\dot{T}| = 10^{-6}/\tau$).

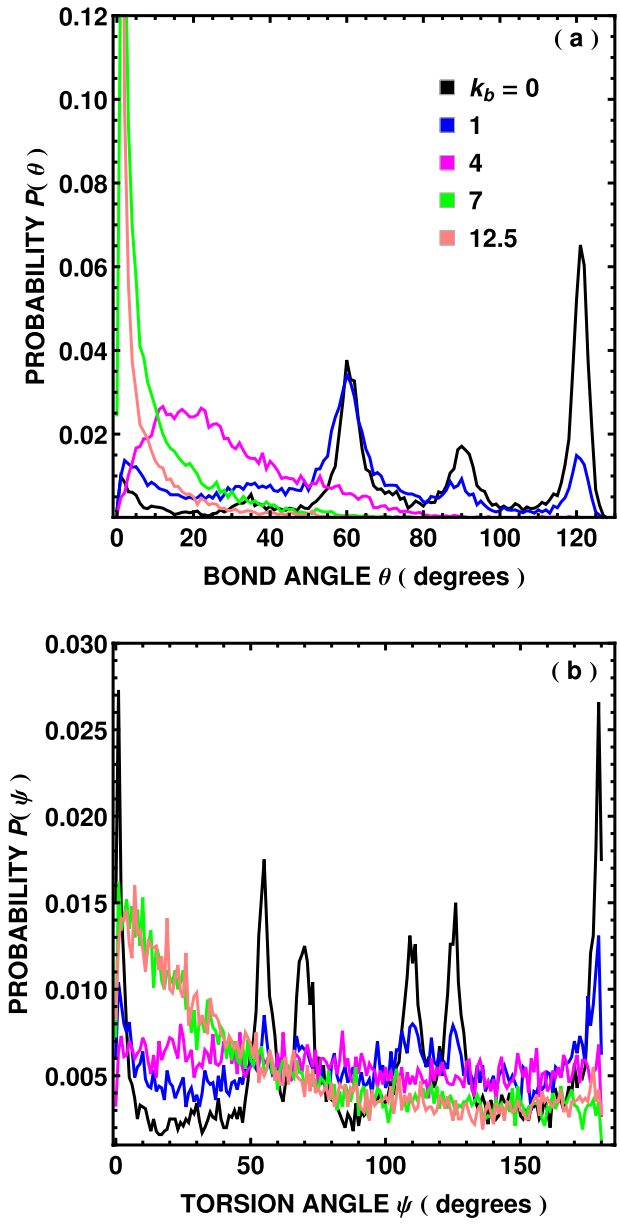

FIG. 4. Probability distributions of (a) bond angles and (b) torsion angles at $T = 0$ for selected $N = 25$ systems. The 0° "origins," respectively, correspond to straight trimers and trans conformers.

both the critical rates for crystal nucleation and growth,[2] and the entropy of close-packed crystallites. Simulations with shorter and longer chains indicate that these trends strengthen with increasing N, especially once N increases beyond the onset of chain entanglement,[31] and especially for stiffer chains.

Angular stiffness effects on local (dis)ordering propensity can be readily examined though analyzing distributions of bond and torsion angles (respectively, θ and ψ). Figure 4 shows the probability distributions $P(\theta)$ and $P(\psi)$ in the $T = 0$ end states of cooling runs for selected k_b. For flexible chains, peaks are in $P(\theta)$ are observed at 0°, 60°, 90°, and 120°, characteristic of a stack-faulted close-packed structure[21] and similar to that observed in crystallized athermal polymers.[34] The peaks characteristic of crystalline order decrease in intensity as k_b increases and vanish by $k_b = 2.5\epsilon$, being replaced by a single broad peak at large θ (e.g., as shown for $k_b = 4\epsilon$). We claim that locally amorphous order arises because this large, broad peak is incompatible with close-packed ordering, e.g., chains are too stiff (flexible) to form the characteristic 120° (0°) angles with high probability at temperatures near solidification. In other words, chains in glassforming systems are too stiff to collapse into random-walk configurations and form close-packed (RWCP) crystals, but not stiff enough to form the extended nematic domains essential for crystallization into the NCP phase. Thus, crystallization is hindered and systems remain amorphous during solidification. As stiffness continues to increase, however, the abovementioned broad peak is replaced by a sharp peak at $\theta = 0°$ (illustrated here in $P(\theta)$ for $k_b = 12.5\epsilon$), indicating increasingly rodlike configurations that can efficiently close-pack and form NCP crystallites.

Torsional angle distributions show consistent trends that reinforce the above hypothesis. Flexible chains show sharp

peaks at $\psi = 0°$, 55°, 70°, 110°, 125°, and 180°. These angles have been shown in previous studies of athermal chains[34] to correspond to collapsed, locally polytetrahedral conformations. As chain stiffness increases, these maxima gradually disappear and are replaced by a single broad maximum. The first maximum occurs at finite ψ for glassforming systems, and at $\psi = 0$ for systems that combine at least some close-packed local with at least intermediate-scale nematic order; cf. Figs. 5 and 6. All of these trends are consistent with the vanishing of polytetrahedral order that is expected for semiflexible chains that cannot easily adopt compact conformations.

D. Local and global nematic ordering

The role of angular stiffness on chain shape is indicated in Figure 5(a), which illustrates the variation of persistence length l_p with k_b as well as its evolution with decreasing T. Systems span the range from the flexible ($l_p/a \sim 1$) limit for small k_b to the rodlike ($l_p/a = N - 1$) limit for $k_b \gtrsim 10\epsilon$. Stiffer chains clearly uncoil and adopt more-extended configurations as T decreases towards T_s; this is expected since the angular potential employed here (Eq. (3)) is minimized for straight chains, and systems remain near thermodynamic equilibrium above T_s.

The same factors that increase l_p also increase chain- and bond-level nematic order. In Figure 5(b), we present results for the temperature dependence of the chain-level nematic order $S_g(T)$. For all T, S_g increases monotonically with increasing k_b (except for $k_b = 7.0$ systems, which are more ordered than $k_b = 8.5$ systems because the multidomain-nematic ordering of the latter reduces S_g; see below). At high $T > T_s$, ordering oscillates because the unentangled chains employed here have high mobility in the melt state. As expected, in the flexible limit, chain end-to-end vectors remain randomly oriented for all T; no significant ordering at this scale takes place upon crystallization into the RWCP phase. Glass-forming systems display similar behavior; large-scale chain configurations get "frozen in" upon vitrification. In sharp contrast, stiffer chains display a dramatic increase in S_g upon cooling as chain-scale order transitions from isotropic to nematic. Indeed, for all but the stiffest chains, the isotropic → nematic transition *drives* crystallization as follows: when chains align, they pack more efficiently, and thus ϕ increases. This densification drives these systems above the characteristic crystallization density $\phi_{cryst}(k_b)$, and crystallization into the NCP phase occurs spontaneously, i.e., $T_{cryst} = T_{ni}$ for $7\epsilon \lesssim k_b \lesssim 10\epsilon$. Very stiff chains (approaching the rodlike limit) exhibit a separate isotropic → nematic transition at temperatures above T_s.

Figure 5(c) shows the temperature dependence of the average bond-level nematic order $S(T)$. S increases upon cooling, indicating increasing *local* alignment of chains at the bond scale. The increase is especially dramatic for NCP-forming systems, but notably, also occurs for glass-forming systems (i.e., they track the increases in l_p), indicating that even the glassforming systems considered here possess a degree of local nematic order, inherited from the melt. The finite value of S in the flexible limit arises from two factors: (i) topological (chain uncrossability) constraints dictate that nearby bonds cannot freely orient with respect to each other, and (ii) in the RWCP crystal, chain segments tend to align preferentially along locally favored directions of their corresponding HCP or FCC crystallites.

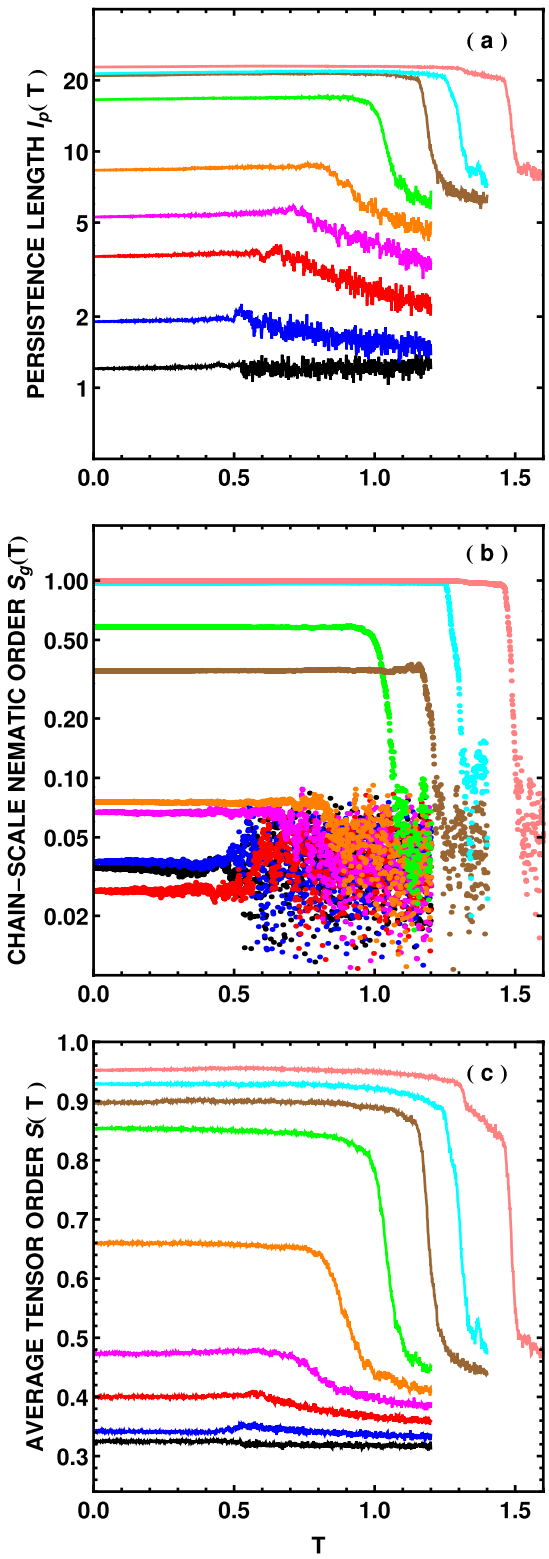

FIG. 5. Thermodynamic signatures of nematic order for selected $N = 25$ systems: (a) persistence length $l_p(T)$ (Eq. (5)), (b) chain-scale nematic order $S_g(T)$ (Eq. (6)), and (c) average tensor order $S(T)$ (Eq. (7)). Colors are the same as in Fig. 2.

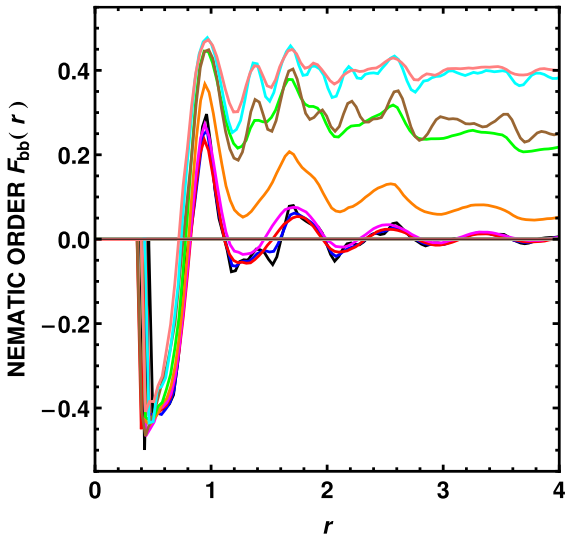

FIG. 6. Nematic order $F_{bb}(r)$ (Eq. (8)) for selected $N = 25$ systems at $T = 0$. Colors are the same as in Fig. 2.

We conclude our discussion of nematic ordering by presenting results for the k_b-dependence of the spatial correlation $F_{bb}(r)$ of the bond-vector orientations. Results for $T = 0$ end states of our cooling runs are shown in Figure 6. All k_b display a "correlation hole" at small r corresponding to the fact that excluded volume prevents dimer pairs from aligning; the closest allowed separation corresponds to a "crossed" configuration which has $F_{bb} = -1/2$. Similarly, in the densely packed systems considered here, dimer pairs separated by approximately one monomer are preferentially aligned. At larger distances, results are highly k_b-dependent. Flexible and glassforming systems exhibit frozen-in, liquid-like order. Long range chain order sets in for $k_b \gtrsim 5\epsilon$ and increases rapidly with increasing k_b until (as discussed further below) aligned chains form a single nematic domain at adequately high k_b values. Finally, note that the onset of mid-range nematic order at $k_b \sim 6\epsilon$ corresponds to the crossover (Table I) from higher to lower values of ϕ_s and ϕ_s^{eff}.

E. (Dis)ordered morphologies formed under cooling; k_b-dependence

Our model exhibits considerably more complexity than might have been surmised, forming a broad array of semicrystalline morphologies. Typical system snapshots of final ($T = 0$) configurations for $N = 25$ systems are shown in Figure 7. In the flexible limit ($k_b \lesssim 1.5\epsilon$), systems freeze into RWCP grains that are randomly shaped and oriented and are separated by twin defects and/or heavily stack-faulted interphases,[21] similar to results from previous studies of fully flexible athermal[34,35,51] chains. In the rod-like limit ($k_b \gtrsim 10\epsilon$), chains tend to form large crystal grains of mixed FCC and HCP character aligned along a single nematic director field, corresponding to close-packed nematic ordering. Defects are also present at the employed cooling rate, for example, the $k_b = 10\epsilon$ system possesses an amorphous interphase that is very similar to the amorphous interlamellar domains typical of semicrystalline synthetic polymers.[2]

In addition to RWCP and NCP crystals and amorphous glasses, we also observe more complex forms of long-range order at intermediate k_b. For $k_b = 8.5\epsilon$ chains form two distinct close-packed grains with different nematic orientations, separated by an amorphous grain boundary. For

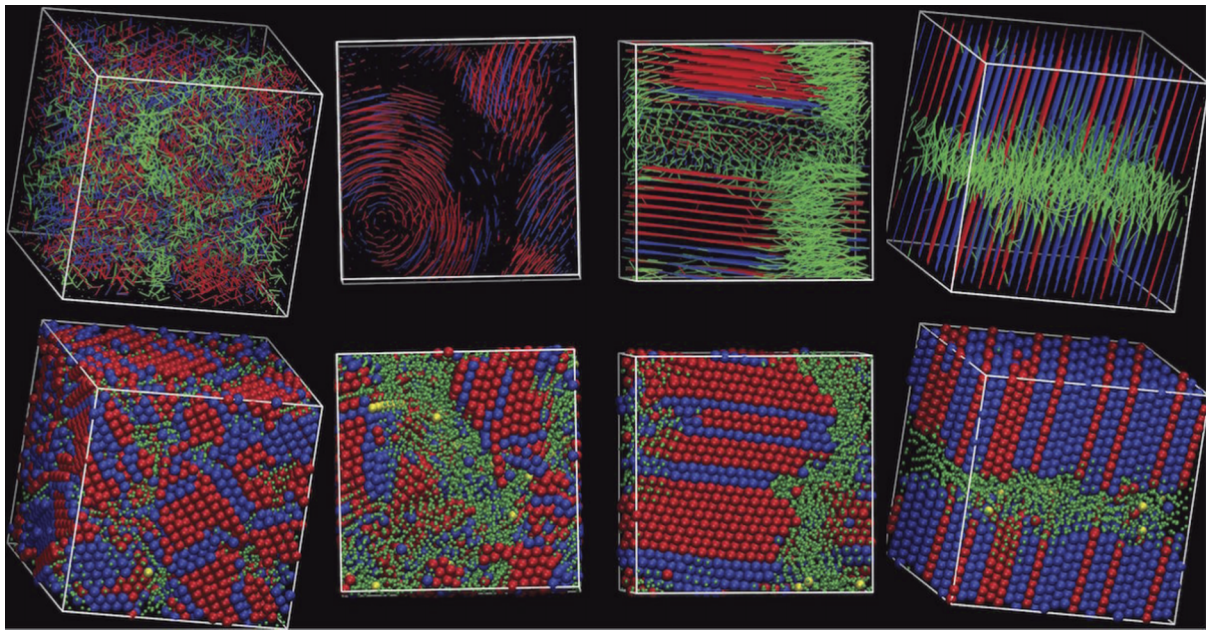

FIG. 7. Snapshots of the $T = 0$ end states of cooling runs for selected $N = 25$ systems. From left to right: $k_b/\epsilon = 0.0, 7.0, 8.5$, and 10.0. In the upper panel, chains shown as lines, while in the lower panel, monomers are shown as spheres. Chain segments/monomers are color-coded according to the CCE-based norm:[38] red, blue, and green, respectively, correspond to FCC-like, HCP-like, and "other" (non close-packed) local environments. The radii of the "other" monomers (in the sphere representation) are reduced for visualization purposes. To more clearly illustrate the spiral, the line representation for $k_b = 7\epsilon$ shows only FCC- and HCP-like monomers. Image created with VMD.[67]

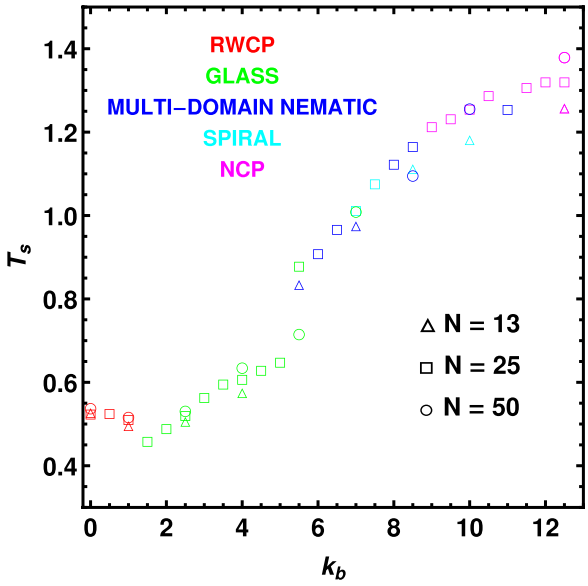

FIG. 8. "Phase" or morphology diagram for this model obtained from simulations at low cooling rate ($|\dot{T}| = 10^{-6}/\tau$), for chain lengths $N = 13$, 25, and 50. Multidomain nematic structure is as illustrated in the Fig. 7 snapshot for $k_b = 8.5\epsilon$.

$k_b = 7\epsilon$, chains form a well-defined spiral morphology. Remarkably, the monomer-level structure is close-packed (possesses HCP and FCC similarity) even near the core of the spiral and remains so as the radial distance from the core increases. At this k_b, the spiral structure forms slightly above T_s, then freezes in upon solidification and serves as a nucleus for close-packed crystal growth. As described in the Appendix, formation of such spirals is quite robust. This structure is similar to those recently observed in experimental and phase-field theory studies of synthetic polymer blends[68–71] and illustrates the wide range of ordered morphologies that can be obtained using simple polymer models with variable chain stiffness.

Next, we present a "phase" diagram for our model. Figure 8 shows both values of T_s and the morphologies formed during solidification, as a function of k_b. Colors and symbol types represent the ordering of the obtained solid phases. For all chain lengths, T_s drops slightly from its flexible-limit value[21] as a small bending stiffness is added ($k_b \lesssim 2\epsilon$), then increases monotonically with increasing k_b; it is worth repeating that while this trend is expected for polymers of increasing stiffness,[54–56] previous studies have not examined models displaying such a broad range of solid-state morphologies. As described above, systems freeze into RWCP crystals for the smallest k_b and single-domain NCP crystals for the largest k_b, while intermediate values of k_b produce either glass-formation or more complex order.

We emphasize that Fig. 8 is *not* an equilibrium phase diagram but rather is simply a representation of k_b-dependent solidification results for the preparation protocol employed here. In particular, the results shown in Fig. 1 indicate that faster cooling rates will expand the range of k_b over which glasses are formed to both larger and smaller values; lower cooling rates will produce opposite trends. Lower $|\dot{T}|$ will also naturally extend the range over which single-domain nematic crystals form to lower values of k_b. A detailed examination of the relative thermodynamic stability of these differently ordered phases would be very interesting but is beyond the scope of the present work.

Nevertheless, at this point it is worthwhile to compare the nonequilibrium results presented in Figure 8 with those that might be "naively" expected (from simple equilibrium-thermodynamic arguments[71]) to be valid in the limit $|\dot{T}| \to 0$. The $T = 0$ ground state for any finite k_b is NCP. As temperature increases, entropy favors adoption of random-walk-like chain structure, and there will be a nematic → isotropic transition at some temperature $T_{ni}(k_b)$ that must increase with increasing k_b.[22,71] This transition must cross the crystallization line $T_{cryst}(k_b)$ at some characteristic value k_b^*. For $k_b < k_b^*$, the thermodynamically stable crystal should be NCP at low T and RWCP at higher $T < T_{cryst}$, while for $k_b > k_b^*$ NCP could plausibly be the only stable solid phase. The nucleation barrier for the RWCP ↔ NCP solid-solid transition will be extremely high, and this transition is not expected to be observed in either simulations or experiments. However, for $k_b \simeq k_b^*$, it is easy to imagine that there is a competition between RWCP and NCP local structure that can suppress the formation of ordered crystalline solids. The results presented in Figure 4 suggest that this competition indeed exists and can be at least partially understood in terms of structure at the Kuhn-segment (i.e., bending and torsion angle) scale.

According to the above "naive" arguments, systems of stiff chains undergoing cooling at a constant rate $|\dot{T}|$ from initial equilibrium isotropic melts will (in the $|\dot{T}| \to 0$ limit) undergo two separate equilibrium phase transitions: an isotropic → nematic liquid-liquid transition at $T_{ni}(k_b)$, followed by the nematic liquid → NCP crystal transition at $T_{cryst}(k_b)$, with $T_{cryst} < T_{ni}$. For intermediate $|\dot{T}|$, the same two transitions will occur, but since they must be nucleated, supercooling into a metastable isotropic liquid will preceed the isotropic → nematic transition, and supercooling into a metastable nematic liquid will precede crystallization.

Figure 9 shows that $k_b = 12.5\epsilon$ systems cooled at $|\dot{T}| = 10^{-6}/\tau$ exhibit strong signatures of the latter behavior. Values of S and ϕ increase sharply (but continuously) in two different regimes; first at $T \simeq 1.47$ (i.e., near T_{ni}) and again for $T \lesssim 1.32 \simeq T_{cryst}$. These increases are clearly strongly coupled, i.e., (increased nematic alignment) ⟷ (increased density). Their *spatial fluctuations* are also strongly coupled. The blue curve shows the Pearson's correlation coefficient

$$C_{S,\phi} = \frac{cov(S,\phi)}{\sigma_S \sigma_\phi}, \tag{9}$$

of spatial fluctuations in S and ϕ, where $cov(S,phi)$ is the covariance of spatial fluctuations in S and ϕ, and (σ_S, σ_ϕ) are their respective standard deviations.[41] $C_{S,\phi}(T)$ clearly exhibits a strong peak near T_{ni}, corresponding to nucleation and initial growth of the nematic liquid phase.

The trends shown in Figure 9 relate closely to a very interesting (but still largely untested) theoretical prediction by Olmsted *et al.*[72] The authors presented a potential explanation for the spinodal kinetics observed during early stage crystallization of some polymer melts.[74] They hypothesized that a metastable liquid phase $\mathcal{ML}$—possessing both different

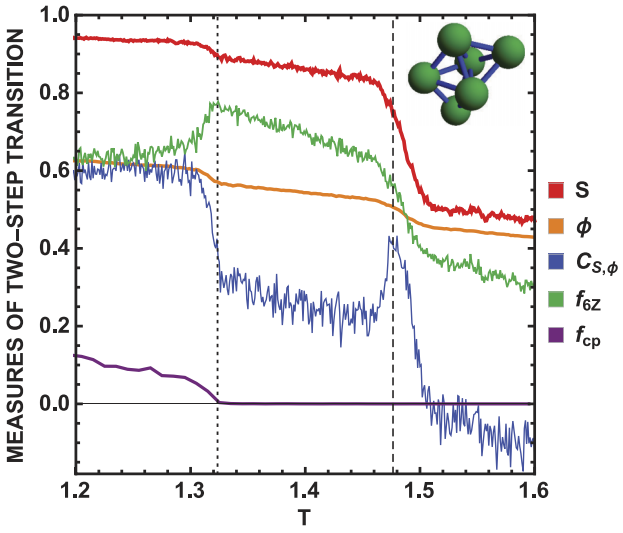

FIG. 9. Two-step transition for $k_b = 12.5\epsilon$ systems. The red, orange, and purple curves, respectively, indicate results for S, ϕ, and f_{cp}. The blue curve indicates the temperature dependence of $C_{S,\phi}$ (Eq. (9)); the peak at $T \simeq T_{ni}$ is consistent with the density-orientation coupling considered by Olmsted *et al.*[72] The green curve indicates the fraction $f_{6Z}(T)$ of atoms belonging to at least one $6Z$[73] cluster (the six-atom cluster with structure shown in the inset). The dotted and dashed vertical lines, respectively, indicate $T_{cryst} \simeq 1.32$ and $T_{ni} \simeq 1.47$ and are included to guide the eye.

symmetry and higher density than the high-T equilibrium liquid phase—forms in the supercooled liquid *prior to* crystal nucleation and growth. If we take $\mathcal{ML}$ to be the supercooled nematic liquid, then behavior fitting the most physically essential part of their hypothesis—that a coupled density-orientation transition between distinct liquid states precedes crystal nucleation—is quite apparent in our Figure 9. However, confirming the predictions of Ref. 72 in any detail would require analyses of relative phase stability that are beyond the scope of this initial study.

Finally, recent simulation studies[73] of colloids have associated key aspects of their glass transition and CF-vs-GF competition with the relative formation propensities of various small, localized "clusters" possessing different structures. One cluster that is particularly relevant to the present work is $6Z$, a six-particle cluster that is one of the two minimal energy clusters for short-range potentials (the other being the octahedron). $6Z$ is incompatible with close-packed order, and its formation propensity has been shown to be closely associated with glass-formability.[73,75] The green curve in Figure 9 shows $f_{6Z}(T)$, the fraction of monomers which belong to at least one $6Z$ cluster. As in crystallizable colloidal systems,[63,76] f_{6Z} rises with decreasing T until the onset of crystallization, then drops sharply, becoming low as f_{cp} becomes large. Of particular note here is the sharp increase of f_{6Z} over the range of T corresponding to the isotropic-nematic liquid-liquid transition. Future work will examine such effects in much greater detail, over a broad range of k_b.

F. Applicability to colloidal polymers

Experimental investigation of the role that chemically specific, microscale interactions play in controlling the (generally nonequilibrium) multiscale structure of synthetic polymer solids — with the aim of establishing predictive relationships — is very difficult. For such studies, CPs composed of chains of linked, macroscopic monomers[23–29] are a promising "proxy system." Their larger size allows far easier observation of their structure on scales ranging from monomers to the bulk, using optical microscopy or even the naked eye.[25] More fundamentally, like their microscopic counterparts, their structural characteristics depend on factors such as chain topology/connectivity, monomer shape, and chain stiffness. For example, the ratio l_K/r_0 is a controllable parameter in CPs,[25,28] and one that can naturally be expected to profoundly affect their bulk morphologies. However, experimental study of CPs remains in its infancy; only a few systems have been synthesized, and the factors affecting their packing at both the monomer and chain scales remain poorly explored.

The various solid morphologies reported here, and in particular, their variation with k_b, may represent a first step towards developing a *qualitative* guide for experiments on real CPs. The obtained morphologies agree with those obtained for athermal polymer models in both the flexible[33–35,51] and rodlike[18] limits, i.e., RWCP and NCP, suggesting that realistic interactions with ranges between the limits of purely repulsive hard spheres and long-ranged-attractive LJ will also produce these morphologies.[77] For example, our results suggest that by tuning the stiffness and employing a suitable preparation protocol such as tapping,[78] crystalline samples of colloidal or granular polymers may be experimentally realized. However, it will be critical to investigate the effects upon ordering of factors such as monomer shape (i.e., deviations from sphericity) and bond geometry (e.g., deviations from $l_0 = r_0$ and different equilibrium bond angles). Recent work on both polymeric and nonpolymeric systems suggest that all of these are likely[29,51,52,79–83] to be very important. The data in Table I should facilitate comparison of our results to systems with different pairwise-interaction ranges.

IV. DISCUSSION AND CONCLUSIONS

In this paper, we described the chain-stiffness dependence of the solid-state morphologies formed by model soft-pearl-necklace polymers. By varying a single interaction parameter (the angular stiffness k_b), we illustrated dramatic effects of chain stiffness on the competition between crystallization and glass formation. In the flexible-chain (small-k_b) limit, monomers occupy the sites of close-packed crystallites while chains retain random-walk-like order. At intermediate k_b, crystallization is suppressed in favor of glass formation. As k_b continues to increase, more complex ordered phases such as spirals are also produced, until long-range nematic chain ordering typical of lamellar precursors sets in as the rodlike limit is approached. The complexity of behavior observed here is particularly remarkable in light of the fact that our model possesses a single, well-defined crystalline ground state (NCP) for finite k_b.

We showed that within this single-parameter model, the controlling thermodynamics and kinetics of solidification

both depend strongly and nontrivially on k_b. Under thermal cooling, relatively flexible chains generally exhibit lower solidification temperatures as well as faster crystallization kinetics (and hence sharper disorder-order transitions) than their stiffer counterparts. These dependences, however, are complex and nonmonotonic in k_b. We associated the glass-formation observed at intermediate k_b with the incompatibility of Kuhn-scale structure (i.e., bond and torsion angles) with close-packing. Other factors are probably also highly relevant, including e.g., competition between formation of RWCP and NCP crystalline phases. Forthcoming work will examine local structure and dynamics in melts above T_s in order to isolate the microscopic mechanisms underlying this complex, k_b-dependent behavior.[81–83]

Since our model's ground state is a close-packed crystal, the results presented herein are likely only indirectly relevant to typical synthetic, semicrystalline polymers such as PE and PVA. These also crystallize and form hexagonal order in planes perpendicular to the nematic director field in both experiments[2] and simulations[8,9,53] but do not form three-dimensional close-packed structures. Furthermore, our preliminary simulations of longer chains have not produced the chain-folded lamellae typical of semicrystalline polymers, perhaps because the lack of torsional interactions removes a necessary thermodynamic driving force for chain-folding; previous work has found that lamella-formation is enhanced by strengthening torsional interactions.[84] However, these issues do not violate the spirit of our modeling effort, which was to isolate the effect of chain stiffness on the crystallization-vs-glass-formation competition, in a minimal model possessing the features (i)-(iv).

Finally, we note that the experimental counterpart to such an approach is very challenging. Synthetic polymer families (e.g., of homologues[2]) which possess each of features (ii)-(iv) are few and far between. Furthermore, it is extremely difficult[22] to isolate the effects of chain stiffness from those of concomitant changes in other factors, such as tacticity, side-chain density, ground-state-structure, and (for copolymers) racemic and chemical composition, that affect the crystallization process as much, or more, as chain stiffness. In light of such challenges, we argue that the present study represents a useful initial step in a long-term effort aimed at improving our understanding of polymer crystallization, glass-formation, and the competition between them, via "minimalist" coarse-grained modeling. Additional features specific to particular chemistries can be progressively added to the model as they are shown to be necessary to capture specific phenomena of interest.

ACKNOWLEDGMENTS

We gratefully acknowledge Wesley R. Burghardt, Nathaniel A. Lynd, and Martin Kröger for helpful discussions. NCK acknowledges support through project "I3" of the Spanish Ministry of Economy and Competitiveness (MINECO) and the computer resources, technical expertise and assistance provided by the Centro de Computacion y Visualizacion de Madrid (CeSViMa).

APPENDIX: FINITE SIZE EFFECTS AND SPIRAL MORPHOLOGIES

Small variations in the initial (high-T) states of samples used in MD quench runs may produce larger differences in their final (low-T) states, especially if k_b is near a phase transition between two different types of k_b-dependent ordering. Here, we discuss how such variations can affect the morphologies produced by our model, focusing on finite-system-size effects. We consider the sample-to-sample variations of $N = 25$, $k_b = 7\epsilon$ systems. Per Figure 8, this value of k_b is in the spiral-forming range, but near the "transitions" to other complex ordered phases. The left panels of Figure 10 shows how the fraction of close packed sites $f_{cp}(T)$ and the global tensor parameter $S_g(T)$ (Eq. (6)) evolve during cooling for three different (but identically prepared) realizations. All three trajectories crystallize at practically identical $T = T_{cryst}$ and $\phi = \phi_{cryst}$. However, the fraction of ordered sites in the final $T = 0$ states differs by approximately 15%, and the nematic order parameter by a factor ~2.5, between the two extreme cases. Very well developed spirals can be observed in the top two "snapshot" panels of Fig. 10,

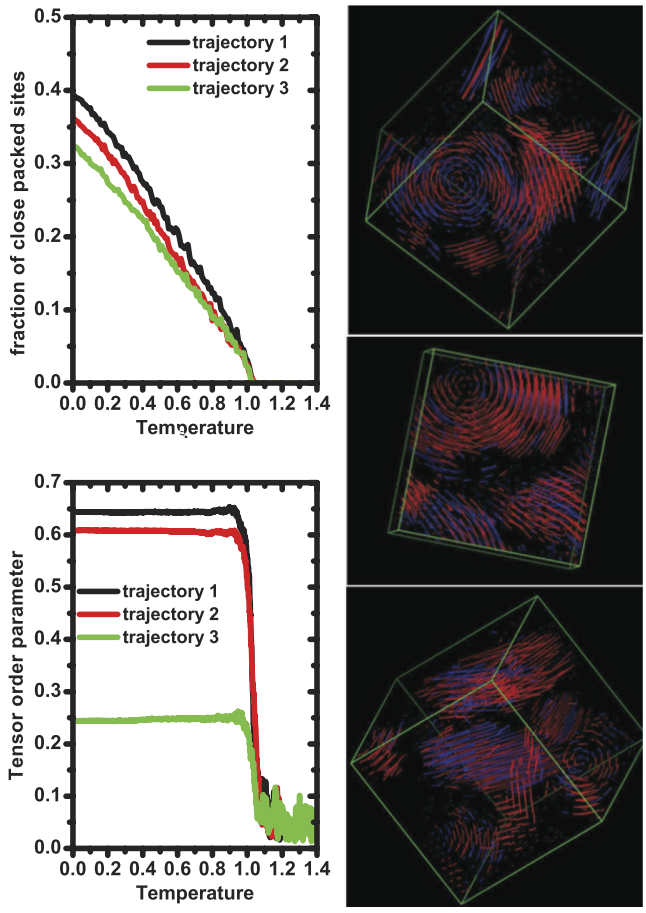

FIG. 10. Finite size effects for $N = 25$ with $k_b = 7\epsilon$ and $|\dot{T}| = 10^{-6}/\tau$. Left panels: fraction of close packed sites f_{cp}, and global tensor parameter S_g (Eq. (6)), versus temperature as obtained from MD runs on three different realizations of $N_{ch} = 500$ systems. Initial configurations were generated using the same protocol. Right panels: Snapshots of $T = 0$ configurations corresponding to these three realizations. Color coding and the "line" representation are the same as Fig. 7, but for clarity, only close packed (HCP or FCC) chain segments are shown.

but in the bottom panel, the characteristic ring of the spiral morphology is less developed, and co-exists with nematic domains. While there are clearly finite-size effects for these systems, these results also make clear that the spiral "phase" is quite robust. Preliminary simulations of much larger systems indicate that the spirals are not the artifacts of the periodic boundary conditions sometimes found in systems under severe confinement.[85]

[1]A. Keller, Rep. Prog. Phys. **31**, 623 (1968).
[2]G. Strobl, *The Physics of Polymers* (Springer, 2007).
[3]M. Doi and S. F. Edwards, *The Theory of Polymer Dynamics* (Clarendon Press, Oxford, 1986).
[4]M. Muthukumar, Eur. Phys. J. E **3**, 199 (2000).
[5]G. Strobl, Rev. Mod. Phys. **31**, 1287 (2009).
[6]J. P. Ryckaert and A. Bellemans, Faraday Discuss. **66**, 95 (1978).
[7]S. Toxvaerd, J. Chem. Phys. **93**, 4290 (1990).
[8]H. Meyer and F. Müller-Plathe, J. Chem. Phys. **115**, 7807 (2001).
[9]H. Meyer and F. Müller-Plathe, Macromolecules **35**, 1241 (2002).
[10]C. Liu and M. Muthukumar, J. Chem. Phys. **109**, 2536 (1998).
[11]P. V. K. Pant, J. Han, G. D. Smith, and R. H. Boyd, J. Chem. Phys. **99**, 597 (1993).
[12]C.-F. Luo and J.-U. Sommer, Phys. Rev. Lett. **102**, 147801 (2009).
[13]J.-U. Sommer and C. Luo, J. Polym. Sci., Part B: Polym. Phys. **48**, 2222 (2010).
[14]C.-F. Luo and J.-U. Sommer, Macromolecules **44**, 1523 (2011).
[15]C.-F. Luo and J.-U. Sommer, ACS Macro Lett. **2**, 31 (2013).
[16]C. Vega, C. McBride, and L. G. MacDowell, J. Chem. Phys. **115**, 4203 (2001).
[17]C. Vega and C. McBride, Phys. Rev. E **65**, 052501 (2002).
[18]H. Fynewever and A. Yethiraj, J. Chem. Phys. **108**, 1636 (1998).
[19]K. Kremer and G. S. Grest, J. Chem. Phys. **92**, 5057 (1990).
[20]C. Bennemann, W. Paul, K. Binder, and B. Düunweg, Phys. Rev. E **57**, 843 (1998).
[21]R. S. Hoy and N. C. Karayiannis, Phys. Rev. E **88**, 012601 (2013).
[22]M. Ballauf, Angew. Chem. **28**, 253 (1989).
[23]M. Z. Miskin and H. M. Jaeger, Nat. Mater. **12**, 326 (2013).
[24]M. Z. Miskin and H. M. Jaeger, Soft Matter **10**, 3708 (2014).
[25]L.-N. Zou, X. Cheng, M. L. Rivers, H. M. Jaeger, and S. R. Nagel, Science **326**, 408 (2009).
[26]S. Sacanna, W. T. M. Irvine, P. M. Chaikin, and D. J. Pine, Nature **464**, 575 (2010).
[27]E. Brown, A. Nasto, A. G. Athanassiadis, and H. M. Jaeger, Phys. Rev. Lett. **108**, 108302 (2012).
[28]H. R. Vutukuri, A. F. Demirors, B. Peng, P. D. J. van Oostrum, A. Imhof, and A. van Blaaderen, Angew. Chem., Int. Ed. **51**, 11249 (2012).
[29]L. Feng, R. Dreyfus, P. Chaikin, and J. Brujic, Soft Matter **9**, 9816 (2013).
[30]R. Auhl, R. Everarers, G. S. Grest, K. Kremer, and S. J. Plimpton, J. Chem. Phys. **119**, 12718 (2003).
[31]R. S. Hoy, K. Foteinopoulou, and M. Kröger, Phys. Rev. E **80**, 031803 (2009).
[32]S. Plimpton, J. Comput. Phys. **117**, 1 (1995).
[33]N. C. Karayiannis, K. Foteinopoulou, and M. Laso, Phys. Rev. Lett. **103**, 045703 (2009).
[34]N. C. Karayiannis, K. Foteinopoulou, C. F. Abrams, and M. Laso, Soft Matter **6**, 2160 (2010).
[35]N. C. Karayiannis, K. Foteinopoulou, and M. Laso, Int. J. Mol. Sci. **14**, 332 (2013).
[36]Z. Zhang, N. Xu, D. T. N. Chen, P. Yunker, A. M. A. Alsayed, K. B. Aptowicz, P. Habdas, A. J. Liu, S. R. Nagel, and A. G. Yodh, Nature **459**, 230 (2009).
[37]As discussed in Ref. 36, there is some freedom of choice in the prefactor of k_BT in Equation (4). Here we have chosen it to be 1.1; other values in the range 1 – 1.2 produce nearly equivalent results.
[38]N. C. Karayiannis, K. Foteinopoulou, and M. Laso, J. Chem. Phys. **130**, 074704 (2009).
[39]P. J. Steinhardt, D. R. Nelson, and M. Ronchetti, Phys. Rev. B **28**, 784 (1983).
[40]P. G. de Gennes, *Scaling Concepts in Polymer Physics* (Cornell University Press, Ithaca, 1979).
[41]For the the purpose of calculating S, simulation cells are divided into $(N_x \times N_y \times N_z)$ cubic sub-cells. We chose $N_x = N_y = N_z = 14$. Note that both S and ϕ can exhibit significant spatial fluctuations during cooling runs; $C_{S,\phi}$ (Eq. (9), Fig. 9) indicates fluctuations among these subcells.
[42]C. F. Abrams and K. Kremer, J. Chem. Phys. **115**, 2776 (2001).
[43]M. E. Mackura and D. S. Simmons, J. Polym. Sci., Part B: Polym. Phys. **52**, 134 (2013).
[44]Note that the K-G model does allow formation of liquid crystalline order when chain stiffness is sufficiently high.[45]
[45]F. Affouard, M. Kröger, and S. Hess, Phys. Rev. B **54**, 5178 (1996).
[46]In the partially flexible (PF) model,[47,48] part of each chain is maintained in a linear configuration (i.e., a rod), and the remainder is completely flexible (freely-jointed). Chain rigidity in the PF model is characterized by the fraction of monomers f_r in the rigid segment, e.g., monomers are arranged into rigid linear rods for $f_r = 1$,[16,17] whereas $f_r = 0$ corresponds to flexible THS. In contrast, chain rigidity in our model is constant along chains and is specified by the strength k_b of angular interactions between three consecutive monomers (Eq. (3)).
[47]B. Oyarzun, T. van Westen, and T. J. H. Vlught, J. Chem. Phys. **138**, 204905 (2013).
[48]T. van Westen, B. Oyarzun, T. J. H. Vlught, and J. Gross, J. Chem. Phys. **138**, 034505 (2013).
[49]N. C. Karayiannis and M. Laso, Phys. Rev. Lett. **100**, 050602 (2008).
[50]N. C. Karayiannis, K. Foteinopoulou, and M. Laso, J. Chem. Phys. **130**, 164908 (2009).
[51]R. Ni and M. Dijkstra, Soft Matter **9**, 365 (2013).
[52]N. C. Karayiannis, K. Foteinopoulou, and M. Laso, Soft Matter **11**, 1688 (2015).
[53]T. Vettorel, H. Meyer, J. Baschnagel, and M. Fuchs, Phys. Rev. E **75**, 041801 (2007).
[54]J. Dudowicz, K. F. Freed, and J. F. Douglas, J. Phys. Chem. B **109**, 21285 (2005).
[55]K. Kunal, C. G. Robertson, S. Pawlus, S. F. Hahn, and A. P. Sokolov, Macromolecules **41**, 7232 (2008).
[56]B. Schnell, H. Meyer, C. Fond, J. P. Wittmer, and J. Baschnagel, Eur. Phys. J. E **34**, 97 (2011).
[57]A. V. Kyrylyuk and A. P. Philipse, Phys. Status Solidi A **208**, 2299 (2011).
[58]S. Torquato, T. M. Truskett, and P. G. Debenedetti, Phys. Rev. Lett. **84**, 2064 (2000).
[59]J. Russo and H. Tanaka, Sci. Rep. **2**, 505 (2012).
[60]M. Leocmach and H. Tanaka, Nat. Commun. **3**, 974 (2012).
[61]J. Taffs, S. R. Williams, H. Tanaka, and C. P. Royall, Soft Matter **9**, 297 (2013).
[62]N. C. Karayiannis, R. Malshe, J. J. de Pablo, and M. Laso, Phys. Rev. E **83**, 061505 (2011).
[63]N. C. Karayiannis, R. Malshe, M. Kröger, J. J. de Pablo, and M. Laso, Soft Matter **8**, 844 (2012).
[64]F. C. Frank, Proc. R. Soc. London, Ser. A **215**, 43 (1952).
[65]F. Trudu, D. Donadio, and M. Parrinello, Phys. Rev. Lett. **97**, 105701 (2006).
[66]H. Wang, H. Gould, and W. Klein, Phys. Rev. E **76**, 013604 (2007).
[67]W. Humphrey, A. Dalke, and K. Schulten, J. Mol. Graphics **14**, 33 (1996).
[68]Y. Okabe, T. Kyu, H. Saito, and T. Inoue, Macromolecules **31**, 5823 (1999).
[69]T. Kyu, H.-W. Chiu, A. J. Guenthner, Y. Okabe, H. Saito, and T. Inoue, Phys. Rev. Lett. **83**, 2749 (1999).
[70]H. Xu, H.-W. Chiu, Y. Okabe, and T. Kyu, Phys. Rev. E **74**, 011801 (2006).
[71]A. M. Donald, A. H. Windle, and S. Hanna, *Liquid Crystalline Polymers* (Cambridge University Press, 2005).
[72]P. D. Olmsted, W. C. K. Poon, T. C. B. McLeish, N. J. Terrill, and A. J. Ryan, Phys. Rev. Lett. **81**, 373 (1998).
[73]A. Malins, J. Eggers, C. P. Royall, S. R. Williams, and H. Tanaka, J. Chem. Phys. **138**, 12A535 (2013).
[74]M. Imai, K. Kaji, and T. Kanaya, Macromolecules **27**, 7103 (1994).
[75]A. Malins, J. Eggers, H. Tanaka, and C. P. Royall, Faraday Discuss. **167**, 405 (2013).
[76]T. Kawasaki, T. Araki, and H. Tanaka, Phys. Rev. Lett. **99**, 215701 (2007).
[77]In experiments, the attractive interactions between colloidal monomers are typically short-ranged, and weak beyond (at most) ~10% of the monomer diameter. Here we have used a Lennard-Jones potential with much longer-ranged attractions (Eq. (1)). One potential objection to use of LJ pair potential to study CPs is that systems with short-ranged attractions exhibit a direct gas-solid transition with only a metastable liquid. However, this difference is largely irrelevant with respect to the applicability of our work to predicting the results of experiments like those typically employed to prepare dense athermal-CP samples;[23–25,27] these create this metastable liquid during sample preparation, i.e., the intermediate-ϕ state in the early stage of a tapping[78] experiment.

[78]J. B. Knight, C. G. Fandrich, C. N. Lau, H. M. Jaeger, and S. R. Nagel, Phys. Rev. E **51**, 3957 (1995).
[79]A. Donev, F. H. Stillinger, P. M. Chaikin, and S. Torquato, Phys. Rev. Lett. **92**, 255506 (2004).
[80]P. F. Damasceno, M. Engel, and S. C. Glotzer, Science **337**, 453 (2012).
[81]A preliminary study of the T-dependence of dynamics in equilibrated $k_b = 4\epsilon$ melts has verified that these systems exhibit Vogel-Fulcher dyamical slowdown and are indeed glass-formers.[82] These results provide an interesting complement to a recent study[83] that employed a (noncrystallizable) KG-like model with variable chain stiffness to study the influence of stiffness on chain packing and fragility[82] in glass-forming systems. A detailed analysis of the relation of such measures of k_b-dependent melt dynamics to (also k_b-dependent) local and long-range order is in progress and will be published separately.
[82]M. D. Ediger, Annu. Rev. Phys. Chem. **51**, 99 (2000).
[83]R. Kumar, M. Goswami, B. G. Sumpter, V. N. Novikov, and A. P. Sokolov, Phys. Chem. Chem. Phys. **15**, 4604 (2013).
[84]N. Lacevic, L. E. Fried, and R. H. Gee, J. Chem. Phys. **128**, 014903 (2008).
[85]G. T. Pickett, M. Gross, and H. Okuyama, Phys. Rev. Lett. **85**, 3652 (2000).